scientific reports

Check for updates

OPEN

Improving the drug delivery performance of ZIF-8 with amine functionalization as a 5-fluorouracil nanocarrier

Sahba Mirzanejad[1], Mojtaba Bagherzadeh[1]✉, Arshad Bayrami[2], Hossein Daneshgar[1], Aida Bahrami[3] & Majid Mahdavi[3]

This study investigates the effect of amine functional groups in ZIF-8 metal–organic frameworks on the loading and release of 5-fluorouracil (5-FU). The facile and cost-effective solvent-assisted linker exchange (SALE) method was used to exchange 2-methylimidazole (2-MIM) linkers with 3-amino-1,2,4-triazole (Atz) in the ZIF-8 structure, which resulted in a synthesis of ZIF-8A with 22, 53, and 74% Atz exchange, respectively. The prepared nanoparticles were characterized by ^{1}H-NMR, XRD, FT-IR, FE-SEM, UV–Vis spectroscopy, and zeta potential analysis. Drug encapsulation efficiency results showed 12% for 5-FU@ZIF-8 which increased to 48% for 5-FU@ZIF-8A(53%). Also, the results of *in-vitro* experiments exhibited the pH-responsive behavior of nanocarriers and slower release for 5-FU@ZIF-8A(53%) compared to 5-FU@ZIF-8. The increase in drug encapsulation efficiency and slower release is due to the presence of the amine functional group in the structure, which improves the host-guest interactions between drug molecules and linkers. Moreover, the MTT assay was performed on MCF-7 and HFF-2 cell lines which revealed that 5-FU@ZIF-8A(53%) exhibited more significant cytotoxicity toward cancer cells while less toxicity toward normal cells compared to 5-FU@ZIF-8. These findings highlight the capability of amine-functionalized ZIF-8 as an effective drug delivery system for 5-FU and demonstrate the potential of the facial and low-cost SALE approach as a promising technique in nanocarrier development.

Keywords Metal–organic frameworks (MOFs), ZIF-8, Drug delivery, 5-Fluorouracil (5-FU), Solvent-assisted linker exchange (SALE)

Administration of conventional anticancer drugs presents several drawbacks, including limited drug solubility, frequent dosing requirements, drug degradation before reaching target organs, nonspecific distribution, lack of selectivity, and insufficient pharmacokinetics[1]. 5-Fluorouracil (5-FU) has been employed for several decades as an anticancer agent for treating stomach, breast, liver, and lung cancer[2]. 5-FU displays cytotoxicity properties by inhibiting the action of thymidylate synthase (TS) or incorporating its metabolites into DNA and RNA structure[3]. However, due to a short half-life (10–20 min), drug resistance, and low specificity of 5-FU, the development of effective drug delivery systems (DDS) is essential to control the rate of drug release, enhance drug affinity, selectivity, and minimize side effects[4,5]. Over the past decades, nanoparticle-based therapeutics such as metallic nanoparticles (ZnO NP, Fe_3O_4 NP, AgO NP, or Au NP), lipidic nanoparticles (liposomes, micelles, vesicles, and solid lipid NP), polymeric nanoparticles (nanospheres, nanocapsules, collagen or dendrimer), and metal–organic frameworks (MOFs) have been utilized in DDS[6–10]. Among various materials evaluated for drug delivery, MOFs exhibit many desired characteristics, such as their structural tunability, which allows for the adjustment of their textural properties for drug encapsulation[11].

MOFs are a class of organic–inorganic hybrid materials that have garnered significant interest across various domains, including gas adsorption/separation[12,13], catalysis[14], energy storage[15], bio-imaging[16], and drug delivery[17] due to their ultrahigh surface area, small particle size, porosity, good biocompatibility and biodegradability, and novel physical and chemical properties with controllable functional groups[18–21].

[1]Department of Chemistry, Sharif University of Technology, PO Box 11155-3615, Tehran, Iran. [2]Department of Chemistry, Faculty of Science, Imam Khomeini International University, Qazvin, Iran. [3]Institute of Biochemistry and Biophysics (IBB), University of Tehran, Tehran, Iran. ✉email: bagherzadeh@sharif.edu

Up to now, different types of MOFs have been studied as drug carriers. Among them, the zeolite imidazolate frameworks (ZIFs) with stability, low toxicity, good biodegradability, and versatile functionality are considered promising candidates for efficient drug delivery and controlled release[22]. Within the broad family of ZIFs, ZIF-8, consisting of tetrahedrally coordinated zinc atoms linked by 2-methyl imidazole (2-MIM), is the most established ZIF material due to its intriguing structural features such as large pores (11.6 Å in diameter connected through apertures of 3.4 Å), high thermal stability and large surface area[23–26]. Notably, the ZIF-8 structure remains unchanged under physiological conditions but decomposes under acidic conditions, which makes it suitable for constructing pH-sensitive DDS[27]. In addition to the aforementioned structural advantages of ZIF-8, the simple preparation of ZIF-8 also reduces the economic cost of healthcare[28]. Table 1 presents some reported ZIF-8 systems for delivering different drugs.

Despite the benefits of the ZIF-8 as DDS, several substantial difficulties still exist. For instance, ZIF-8 nanoparticles demonstrate low affinity for certain drugs, resulting in reduced loading capacity and undesired premature release of drugs[29]. Additionally, high concentrations of ZIF-8 nanoparticles have been shown to cause toxicity; therefore, their doses must be limited[30]. Various methods have been examined to improve the ZIF-8 drug delivery system and address existing challenges. One strategy involves surface modifications with functional molecules, including polydopamine (PDA), polyethylene glycol (PEG), hyaluronic acid, and silica, which have been successfully utilized for the surface functionalization of ZIF-8 nanoparticles to upgrade their stability and biocompatibility[31–34]. Qiong Wuand et al. modified the ZIF-8 surface by coating it with PDA to reduce toxicity[35]. Liuhui Su et al. also enhanced the biocompatibility of nanocarriers by coating ZrO_2 on the surface of ZIF-8[36]. However, surface modifications often block the pore size of ZIF-8 and lead to decreased drug loading capacity[37]. Another promising strategy is conjugating targeting agents such as folic acid (FA), aptamers, monoclonal antibodies, and peptides to facilitate the delivery of the system to cancer cells and reduce off-target effects[38]. Reshmi's group modified the ZIF-8 surface through amination and then conjugated it with folic acid due to its high affinity for the folate receptor (FR), which is overexpressed in cancer cells[39]. Although FA molecules quickly permeate tissues and reach the target owing to their small size, FR is also expressed in several normal tissues, which can cause off-target effects[40]. On the other hand, monoclonal antibodies as targeting agents offer higher specificity, whereas the risk of immunogenic reactions might increase[41]. Generally, surface modification is challenging due to harsh reaction conditions and high production costs, making scaling up difficult. These methods often fail to improve the affinity between drug molecules and nanocarriers[29]. Ensuring a high drug encapsulation efficiency reduces the amount of nanocarriers needed to reach the therapeutic level, minimizes side effects, and decreases the manufacturing cost of nanomedicine. Therefore, developing strategies to improve drug loading is urgent[42].

One promising approach to improve drug encapsulation and overcome these issues is the solvent-assisted linker exchange (SALE) method, which offers the possibility of exchanging original linkers with another possessing new functionality, thereby enhancing the affinity between the drug and the nanocarrier. Conceptually, the SALE process occurs at the solid-solution interface. A parent MOF is immersed in a solution containing a second linker, leading to the formation of a daughter MOF that shares the same topology as the parent MOF[43]. To the best of our knowledge, it is the first time that amine-functionalized ZIF-8 is considered a potential nanocarrier. In this study, we employed the cost-effective SALE method to exchange 2-MIM with 3-amino-1,2,4-triazole (Atz) in ZIF-8 frameworks, investigating the effect of the amine functional group on drug loading and controlled release. For this purpose, three amine-functionalized ZIF-8 with 22, 53, and 74% of Atz exchange were prepared, and a drug model 5-FU was encapsulated into prepared materials (Fig. 1). The pH-responsive release behavior of selected samples was examined at pH 5 (acidic conditions) and pH 7.4 (physiological conditions). Finally, the MTT assay was performed in MCF-7 and HFF-2 cell lines to evaluate the cytotoxicity of samples. Our findings highlight the potential of ZIF-8A(53%) as a suitable carrier for 5-FU.

Experimental

Materials and characterization method

Materials

All reagents and solvents were commercially available and used without further purification. Zinc nitrate hexahydrate (98%), 3-amino-1,2,4-triazole (Atz, ≥ 95%), 2-methylimidazole (2-MIM, 99%), disodium hydrogen phosphate dihydrate (99.9%), sodium phosphate monobasic (99%), methanol (99.9%), sodium hydroxide

MOF	Modifications	Loaded drug	Stimulus	Application	Ref
Cur@ZIF-8@HA	Coated by hyaluronic acid (HA)	Curcumin (Cur)	pH-responsive	Breast cancer-4T1 cell treatment	33
ZIF-8@DOX@organosilica	Modified by organosilica	Doxorubicin (DOX)	pH and redox dual-responsive	HeLa and MCF-7 cell treatment	34
FA-PEG/CQ@ZIF-8	Modified by methoxy poly(ethylene glycol)-folate (FA-PEG)	Chloroquine diphosphate (CQ)	pH-responsive	Autophagy inhibitor-HeLa cell treatment	44
PDA/MTX@ZIF-8	Modified by polydopamine (PDA)	Methotrexate (MTX)	pH and NIR-responsive	Chemo-photothermal therapy- MG63 cell treatment	45
Di-PEG@PTX@ZIF-8	Modified by peptide dimer (Di-PEG)	Paclitaxel (PTX)	pH-responsive	Prostate cancer- Lncap cell treatment	46
Fe_3O_4@PAA@ZIF-8@CIP	Modified by Fe_3O_4@PAA	Ciprofloxacin (CIP)	pH-responsive	Antibacterial activity	47
CBP@ZIF-8	–	Carboplatin (CBP)	pH-responsive	A549 cell treatment	48

Table 1. Reported ZIF-8 composites containing various loaded drugs and their applications.

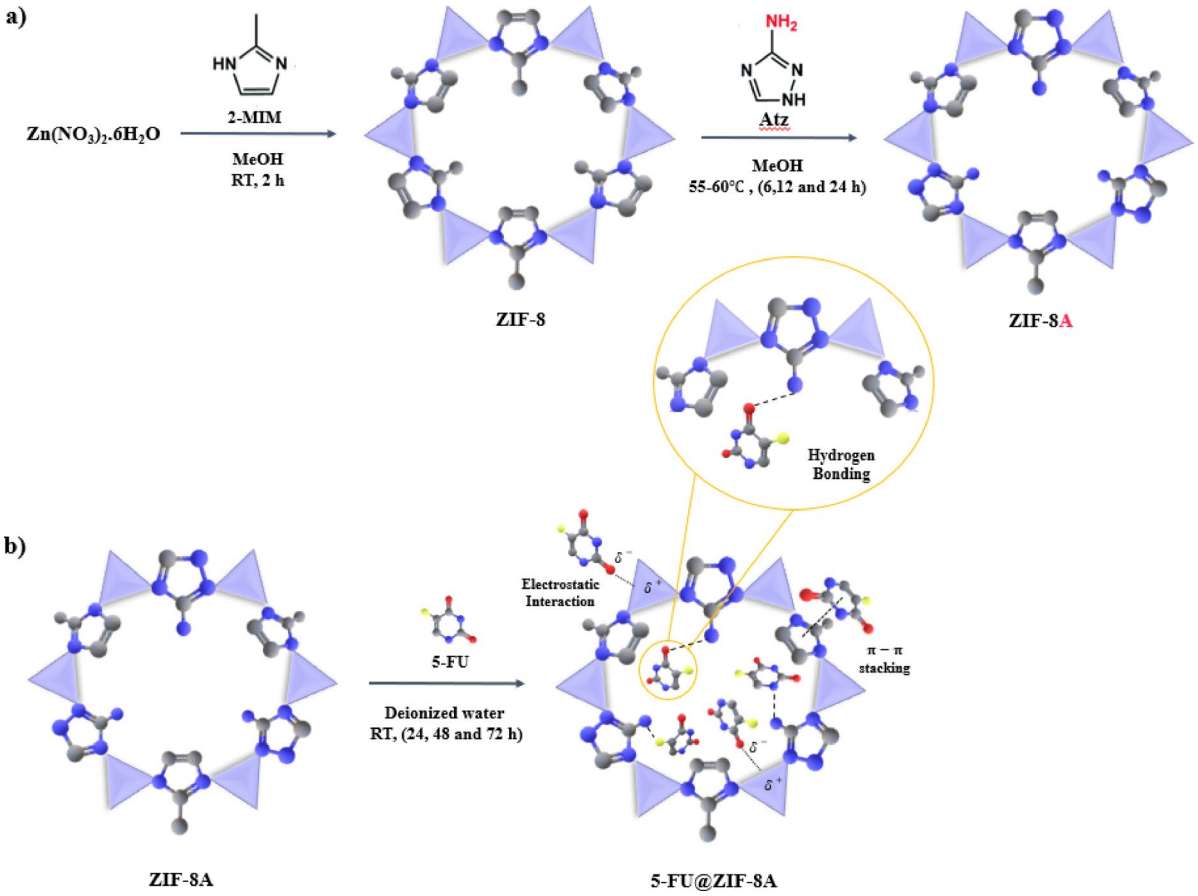

Fig. 1. (**a**) Synthesis procedure for ZIF-8 and amine-functionalized ZIF-8 (ZIF-8A); (**b**) Encapsulation procedure for ZIF-8A along with possible host–guest interactions (hydrogen bond formed between the hydrogen atom of the amine group and the functional groups of 5-FU, π–π stacking, electrostatic interaction).

(NaOH, 99.9%), and sulfuric acid (H_2SO_4, 98%) were obtained from Sigma Aldrich. 5-Fluorouracil (5-FU) 250 mg/5 mL was purchased from FAREVA Unterach GmbH. Deuterated dimethyl sulfoxide (DMSO-d_6, 99.9%) was used as the solvent for NMR analysis.

Characterization method

^{1}H-NMR spectra were acquired at 25 °C on a Bruker Avance (400 MHz) spectrometer. The ^{1}H-NMR spectra of nanoparticles were obtained by dissolving samples in a dilute mixture of H_2SO_4/DMSO-d_6 (1:9, v/v), aiming to calculate the percentage of linker exchange. Fourier transform infrared spectroscopy (FT-IR) of samples was measured in the wavenumber range of 400–4000 cm^{-1} with a Perkin Elmer (spectrum two) FT-IR spectrometer utilizing the KBr tablet. X-ray diffraction (XRD) patterns of the prepared materials were characterized by Philips Xpert Pro diffractometer system in a range of 2 θ = 5–35° using a Cu K α radiation source (λ = 1.5406 Å). The field emission scanning Microscope (FE-SEM) images were recorded using the TESCAN (MIRA 3 LMU) device equipped with energy-dispersive X-ray spectroscopy (EDX). The UV–Vis spectra were obtained by Cary100Bio spectrophotometer. Zeta potential (ZP) analysis was performed with the ZN series instrument. The *in-vitro* release experiments in phosphate buffer were carried out using the CPR shaker incubator.

Preparation of ZIF-8

ZIF-8 was prepared by following a previously reported procedure with minor modifications[49]. In brief, 9.7 mmol of $Zn(NO_3)\cdot 6H_2O$ (2.9 g) and 84 mmol of 2-methylimidazole (6.9 g) were dissolved separately in 100 mL methanol, respectively. The 2-MIM solution was poured into the zinc solution under vigorous stirring for 2 h at room temperature. The white precipitate was separated by centrifugation and purified by washing three times with methanol. Afterward, the purified ZIF-8 product dried at 80 °C for 48 h.

Preparation of amine-functionalized ZIF-8 (ZIF-8A)

Amine-functionalized ZIF-8 nanoparticles were synthesized by exchanging 2-MIM with Atz through the SALE method. According to the following reported procedure[50], 200 mg of the synthesized ZIF-8 was dispersed in 100 mL methanol using sonication for 25 min. Then 585 mg Atz was added to the ZIF-8 suspension. The SALE method was performed for a specific reaction time at a range temperature of 50–60 °C; 6, 12, and 24 h for 22, 53, and 74% of Atz exchange, respectively. For purification, the obtained products were acquired by

centrifugation and washed three times with methanol. Eventually, nanoparticles were dried at 80 °C for 48 h, and the ultimate products were designated as ZIF-8A(22%), ZIF-8A(53%), and ZIF-8A(74%) owing to linker exchange percentage.

Preparation of phosphate buffer

The Supplementary Information file details the preparation of phosphate buffer used for the in-vitro release experiments.

Drug loading

For integrating 5-FU drug into MOFs, the subsequent procedure was implemented: 10 mg of intended nanoparticles were dispersed in 4 mL deionized (DI) water by sonication for 10 min. Afterwards, 300 µL of stock solution (containing 50 mg/mL 5-FU) was diluted with 700 µL DI water and added to the solution. Then, the final solution was blended three times (24, 48, and 72 h) under magnetic stirring at room temperature. Subsequently, the impregnated MOFs were recovered by centrifugation, rinsed with DI water, and dried for 48 h at 40 °C. The resultant supernatants were collected to analyze drug encapsulation efficiency using UV–Vis spectroscopy. The concentration of 5-FU in supernatant was determined by its absorbance peak measured at 267 nm. The drug loading content (DLC%) and drug encapsulation efficiency (DEE%) were calculated using the equations below[51].

EQUATION NOT FOUND

EQUATION NOT FOUND

In-vitro drug release study

Two different pH solutions of phosphate buffer (pH 5 and 7.4) were used to evaluate the pH-responsive behavior of nanoparticles using the Direct addition method[52]. Initially, 9 mg of each sample separately was immersed in 9 mL phosphate buffer at pH 7.4 (physiological pH conditions) in a 10 mL Falcon tube, then placed in a shaker incubator with 140 rpm at 37 °C (i.e., human body temperature). At specified time intervals, 3 mL of supernatant was withdrawn and replaced immediately by an equal volume of fresh phosphate buffer in order to maintain sink conditions and prevent drug saturation in the release medium[53]. Each time, the collected supernatant was centrifuged, and the clear supernatant was used to determine the cumulative release percentage of 5-FU through UV–Vis spectrophotometer, compared with a calibration curve of free 5-FU. The identical experimental procedure was carried out at pH 5 (acidic pH conditions). The concentration of released drug was obtained according to the standard curve, and the release percentage was calculated using the following equation[51,54]

EQUATION NOT FOUND

Cell culture

The human breast cancer cell line, MCF-7 and normal human skin fibroblast, HFF-2 cells, as normal cell line, were cultured in RPMI 1640 medium containing 1% V/V Penicillin /Streptomycin and 10% fetal bovine serum (FBS) in a humidified atmosphere of 5% CO_2 at 37 °C. Both cell lines were purchased from the Pasteur Institute of Iran (Tehran). The cell culture medium (RPMI 1640), fetal bovine serum (FBS), and Penicillin streptomycin were provided from Gibco (Life Technologies, USA). Methylthiazolyldiphenyl-tetrazolium bromide (MTT) was supplied from Life Biolab (Heidelberg, Germany), and Dimethyl sulfoxide (DMSO) from Merck (Germany).

Cell viability assay

Cell viability is colorimetrically assessed by the MTT reagent. MCF-7 and HFF-2 cells were seeded at a concentration of 1×10^4 cells/well and were treated with each compound (0.5–150 µg/mL), then incubated for 72, 48, and 24 h. Notably, the primary stock solutions of each compound were prepared using DMSO, while its final concentration was kept below 1% in all treatments. After incubation time, 20 µL of the MTT reagent was added to each well, followed by a 3 h incubation. Once the medium was removed, the purple formazan crystals were solubilized by adding 170 µL of DMSO to each well, followed by an hour of incubation at 37 °C or low-speed shaking. The absorbance value of the formazan product was measured at 570 nm using the ELISA reader.

Statical

The IC50 values of compounds, defined as 50% growth inhibition compared to untreated cells, were calculated by the sigmoidal dose–response graph using GraphPad Prism 9.0.0 software. Results were considered statistically significant at the *p*-value of < 0.01 (**), < 0.001(***), < 0.0001(****) and ns: no significant.

Results and discussion

Characterization of prepared MOFs

The prepared nanoparticles were characterized with various analyses. As shown in Fig. 2a, the ^{1}H-NMR spectrum of ZIF-8 displayed peaks at 2.7 (a) and 7.4 ppm (b,b′) which ascribed to methyl and methine groups of 2-MIM, respectively. As a result of the SALE method, the attained product exhibited an additional peak at 8.2 ppm (c) corresponding to the methine peak of Atz, indicating the formation of ZIF-8A. The intensity of the additional peak increased progressively as the reaction time was extended. Atz exchange percentage was evaluated by calculating the intensity ratios of the methine peaks between (b) and (c) from ZIF-8 and ZIF-8A. Based on the obtained ^{1}H-NMR spectra, three ZIF-8A series with 22, 53, and 74% of Atz linker were synthesized after the reaction duration of 6 h, 12 h, and 24 h, respectively[23].

The FT-IR analysis was performed to study functional groups and chemical bonds of synthesis nanoparticles. As depicted in Fig. 2b, the spectrum of bare ZIF-8 represented characteristic peaks, including ZnN stretching at 423 cm^{-1}, C–N stretching at 1180 cm^{-1}, C=N stretching at 1580 cm^{-1}, and C–H stretching at 3135 cm^{-1}[55,56]. The spectra of amino-functionalized ZIF-8, in addition to all the bands in pure ZIF-8, exhibited peaks at 3210, 1052 and 3430, 3370, 1623 cm^{-1}, corresponding to –NH and $–NH_2$ in Atz, respectively. Furthermore, the peaks of N–C–NH, $C–NH_2$, and C=N–NH at 1212, 1518, and 1545 cm^{-1} demonstrated a stronger intensity with increasing Atz exchange, confirming that SALE is indeed appropriate for the synthesis of ZIF-8A[49]. Moreover, the FT-IR spectra of ZIF-8 and ZIF-8A(53%) before and after drug loading were collected to investigate any differences in chemical bonding imparted by 5-FU incorporating. As shown in Fig. 2c, characteristic peaks of 5-FU (free drug) were observed at 3000–3500, 1650, and 1242 cm^{-1}, corresponding to -NH stretching, C=O, and –CF bond, respectively.[57] Owing to the encapsulation of drugs inside the ZIF-8 frameworks, the bands of 5-FU were concealed. Meanwhile, an increased intensity at 1650 and 3000–3500 cm^{-1} in impregnated MOF could be ascribed to C=O, –CF of 5-FU, which indicated a successful loading. Based on previous reports[58,59], the hydrogen bonds can affect the IR spectra, including band broadening, shifting, or intensification. A slight blue shift in the C=O stretching bands of 5-FU and a red shift in the N–H stretching band of the frameworks show the formation of host–guest hydrogen bonding interactions. However, due to the relatively low drug loading amount, these shifts are not sharply resolved and appear as broadened features in the spectra. The observed intensification at 1650 and 3000–3500 cm^{-1} in the drug-loaded MOFs can be attributed not only to the presence of 5-FU but also indicates the formation of hydrogen bonds between drug molecules and frameworks. These changes in band intensity confirm hydrogen bond formation, even without significant shifting. It is worth mentioning that a rise in intensity of 5-FU distinct peaks was more significant in ZIF-8A(53%) due to a higher amount of drug encapsulation.

The crystal structure of the synthesized materials was examined using XRD analysis to prove the formation of the intended structure. As shown in Fig. 3a, the XRD pattern of ZIF-8 exhibited characteristic peaks at 2θ values of 7.2°, 10.3°, 12.5°, 14.5°, 16.4° and 18.0°, which assigned to crystal planes of (011), (002), (112), (022), (013), and (222), respectively (JCPDS card no. 00-062-1030)[60]. Furthermore, the pattern of amine-functionalized ZIF-8 (ZIF-8A(22%), ZIF-8A(53%), and ZIF-8A(74%)) displayed identical peak positions with as-synthesized ZIF-8, indicating that the frameworks have preserved a high level of crystallinity[23]. However, the XRD pattern of ZIF-8A series showed that at a high amount of Atz exchange, the intensity of certain peaks attributed to crystal planes like (002), (112), and (222) diminishes, and broadening appears, implying that the crystallinity is slightly lowered with a high Atz exchange. As depicted in Fig. 3b, the XRD pattern of 5-FU@ZIF-8 and 5-FU@ZIF-8A(53%) revealed similar characteristic peaks with pristine MOFs, confirming that the encapsulation approach did not impact the crystalline structure.

The FE-SEM and EDX analyses were also conducted to investigate the prepared materials' morphology, particle size, and elemental composition. The corresponding images presented in Fig. 3c revealed that ZIF-8A nanoparticles demonstrated a smoother surface compared to ZIF-8 with well-defined hexagonal morphology. Meanwhile, the morphology of ZIF-8 and ZIF-8A(53%) nanoparticles remained unchanged after loading of 5-FU. Furthermore, the particle size distributions obtained from FE-SEM show an average particle size of 50 to 100 nm for all samples. Moreover, EDX spectra and elemental mapping analysis were performed to explore the elemental composition and distribution within the nanoparticles. As expected, EDX spectra of prepared MOFs comprised C, N, and Zn elements (Fig. S1). Results obtained from the EDX spectra indicate that both 5-FU@ZIF-8 and 5-FU@ZIF-8A(53%) contain O and F elements, in addition to the atoms present in the pristine nanomaterials, which are attributed to 5-FU. Further evaluation via elemental mapping disclosed the uniform distribution of O and F elements in drug-loaded samples, suggesting that 5-FU is uniformly distributed throughout the nanocarrier (Fig. S2)[61].

The zeta potential was measured in an aqueous solution to determine the surface charge of the ZIF-8 and ZIF-8A(53%) samples before drug loading. The ZP value of ZIF-8 was + 28.5 mV, whereas that of ZIF-8A(53%) was + 54.7 mV, owing to the presence of amine functional groups, which lead to a more positive surface charge (Fig. S3)[62]. Based on previous report, the 5-FU has a negative ZP value, which expected to result a stronger electrostatic interactions between 5-FU and ZIF-8A(53%) with more positive ZP value[63]. Therefore, the obtained ZP values could also confirm the higher drug loading efficiency of ZIF-8A(53%) compared to ZIF-8.

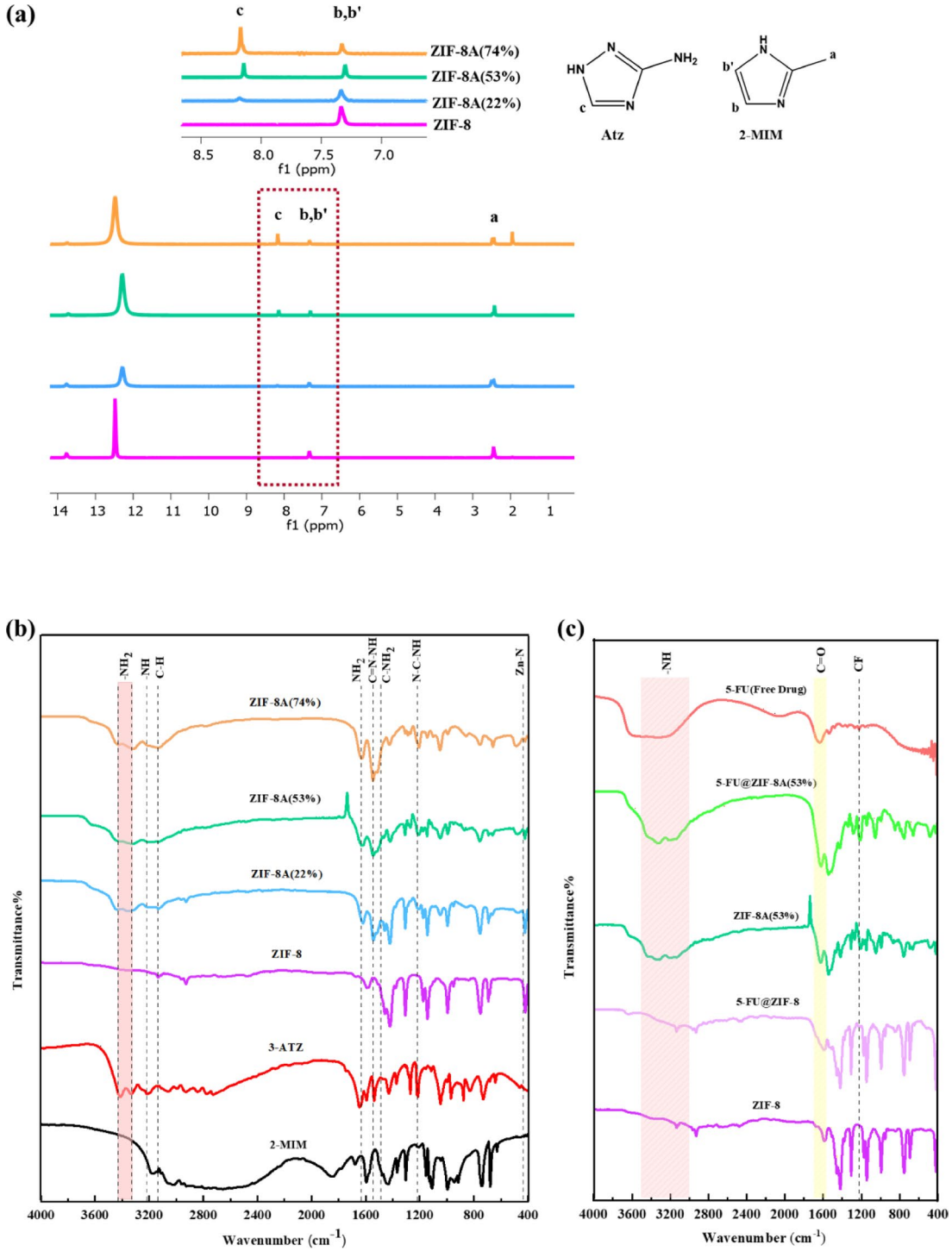

Fig. 2. (**a**) ^{1}H-NMR spectra of ZIF-8 and ZIF-8A with different Atz exchange percentages; (**b**) FT-IR spectra of 2-MIM, Atz, ZIF-8, ZIF-8A(22%), ZIF-8A(53%), and ZIF-8A(74%); and (**c**) FT-IR spectra of 5-FU (Vial), ZIF-8, 5-FU@ZIF-8, ZIF-8A(53%), and 5-FU@ZIF-8A(53%).

Drug loading and release study

The drug encapsulation efficiency and drug loading content values for prepared materials were assessed by UV–Vis spectroscopy based on the distinct peak of 5-FU at 267 nm. In the case of as-synthesized ZIF-8 and ZIF-8A, no characteristic absorbance peaks were observed in the range of 200–800 nm. The UV–Vis spectra of 5-FU before and after loading for intended nanoparticles were illustrated in Fig. S4. Notably, to reach the highest drug loading amount, various factors could be affected, including solvent, relative ratio of 5-FU to porous material, and reaction time. Therefore, DI water was used as a non-toxic solvent in this study. Additionally, the optimal value for the 5-FU to ZIF-8 ratio was considered 3:2, based on previous report[24]. Eventually, three different times

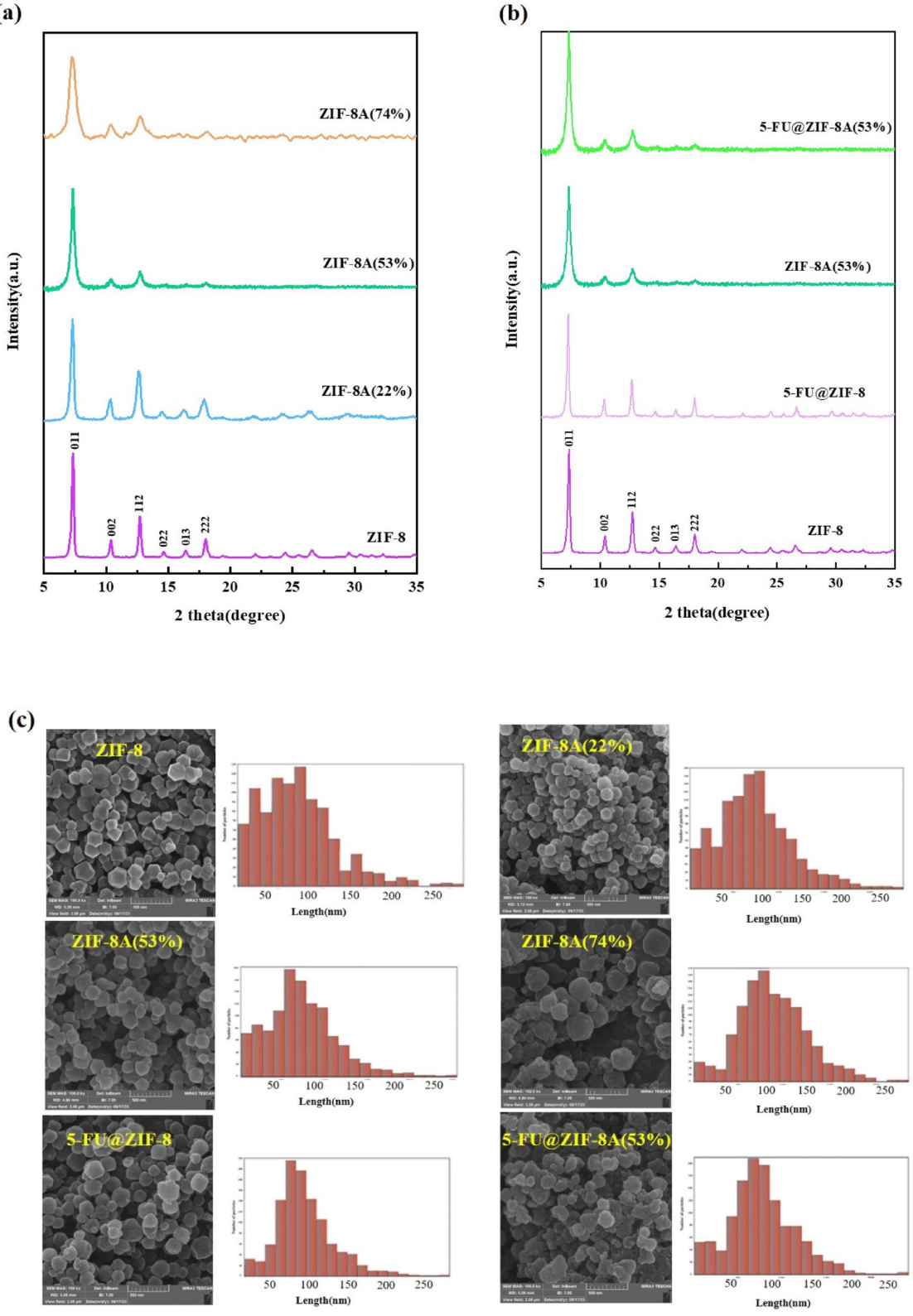

Fig. 3. (**a**) XRD patterns of ZIF-8, ZIF-8A(22%), ZIF-8A(53%), and ZIF-8A(74%); (**b**) XRD patterns of ZIF-8, 5-FU@ZIF-8, ZIF-8A(53%), and 5-FU@ZIF-8A(53%); (**c**) FE-SEM images of ZIF-8, ZIF-8A(22%), ZIF-8A(53%), ZIF-8A(74%), 5-FU@ZIF-8, and 5-FU@ZIF-8A(53%). In some cases, baseline-subtracted XRD patterns were used to make a clearer comparison.

(24, 48, 72 h) were selected to investigate the loading capacity of nanoparticles by varying the loading time. The obtained data is shown in Table 2. The highest drug encapsulation efficiency of 48% was achieved for ZIF-8A(53%) after 24 h, which is significant compared to ZIF-8 with a drug encapsulation efficiency of only 12% after 24 h. According to previous report, the pore volume of ZIF-8A samples experienced a gradual decrease as the Atz linker amount increased[23]. Despite a reduction in pore volume, the existence of several amine-functionalized cavities suggested a possible interaction between the drug molecule and the amine group. The subsequent analysis of drug loading results revealed that in ZIF-8A(53%), both mentioned factors reach a balance and lead to enhanced drug loading. However, probably in ZIF-8A(74%) due to the reduction of pore volume factor, and in ZIF-8A(22%) due to the limited number of amine-functionalized cavities, the drug loading did not exhibit a noticeable difference compared to ZIF-8. Noteworthy, as apparent from DEE results, the optimal loading time for ZIF-8A(53%) was 24 h, and then loading efficiency decreased with time and reached 31% after 72 h. Thus, to investigate the effect of the amine functional group on the release behavior and MTT assay of nanocarrier, ZIF-8 and ZIF-8A(53%) with 12% and 48% DEE, respectively, were selected for further study and comparison.

The pH-responsive release of 5-FU from selected samples was examined in phosphate buffer solutions at pH 7.4 and 5 at 37 °C. The release profile for ZIF-8 indicated the rapid release of 5-FU (about 46%) after 90 min at pH 5, and then the release amount reached a maximum value of 65% after 10 h. In addition, at pH 7.4, approximately 44% of 5-FU was released during the first 90 min, and no further release was observed after that (Fig. 4a). The ZIF-8A(53%) release profile exhibited that around 60% of 5-FU was released after 20 h at pH 5. Moreover, at pH 7.4, the release rate of 5-FU was about 46% after 6 h (Fig. 4b). The burst drug release at initial hours could be due to the weak interactions of absorbed 5-FU molecules on the framework surface. The other drug molecules entrapped with stronger interaction in the pores and cavities of ZIF-8 were released at a slower rate[64]. It is worth mentioning that the electron-rich 5-FU molecules could provide strong host–guest interactions such as hydrogen bonds between drugs and linkers (O–H···O, N–H···O, O–H···F, C–H···π, and N–H···π), π–π stacking, and coordination binding. These interactions significantly promote the loading of 5-FU but, at the same time, delay its release from the pores[61]. According to the obtained results, the release of 5-FU under acidic conditions was more effective than under neutral conditions, indicating the pH-responsive properties of both nanocarriers. The pH sensitivity of ZIF-8 arises from the coordination bonds formed between its metal ions and linkers. In methanol (MOF synthesis condition), 2-methylimidazole undergoes deprotonation, losing an H^+ ion to generate the imidazolate ion, which coordinates with Zn^{2+} ions via nitrogen atoms. Under acidic conditions, the linkers become protonated, leading to the disruption of these coordination bonds. This occurs because both protons and Zn^{2+} ions, as Lewis acids, compete to bind the linker, which acts as a Lewis base[44]. Similarly, the decomposition of ZIF-8A(53%) under acidic conditions can be attributed to the protonation of mixed linkers, 2-MIM and Atz. Furthermore, ZIF-8A(53%) demonstrated slower and sustained release of 5-FU compared to ZIF-8 (Fig. 4c,d). The prolonged release of 5-FU from ZIF-8A(53%) was owing to improved host–guest interaction between the drug and nanocarrier[65]. Notably, considering the same duration of time, the amount of the drug liberated from ZIF-8A(53%) is much higher than ZIF-8 due to the higher drug encapsulation efficiency. Drawing upon the herein results, ZIF-8A(53%) is a promising pH-responsive drug delivery system.

Cytotoxicity assay

MOF drug delivery systems cytotoxicity is commonly evaluated using colorimetric assays that depend on viable cells with active metabolism. These methods include MTT, MTS, fluorescent resazurin-based assays, and CCK-8. Such assays involve co-incubating cell lines with DDS and assay components to evaluate cellular metabolic activity by reducing formazan-related compounds. The emission or absorption, which corresponds to the number of viable cells post-treatment, is measured using a plate reader; any disruption in formazan formation can influence the accuracy of assays such as MTT, CCK-8, and MTS assays[66,67]. In this study, to evaluate the effects of 5-FU@ZIF-8 and 5-FU@ZIF-8A(53%) on cell viability, MTT assay was conducted on MCF-7 and HFF-2 cell lines, also using 5-FU as a positive control. Moreover, to examine the safety of prepared nanocarriers, the cell viability of ZIF-8 and ZIF-8A(53%) was assessed on the HFF-2 cell line. For this purpose, six different concentrations of 5-FU@ZIF-8 and 5-FU@ZIF-8A(53%) nanocarriers, ranging from 5 to 150 µg/mL, were tested

MOFs	Loading time(h)	DEE(%)	DLC(%)
ZIF-8	24	12.0	18.0
	48	11.8	17.7
	72	17.4	26.0
ZIF-8A(22%)	24	8.9	13.4
	48	11.9	17.8
	72	16.0	24.0
ZIF-8A(53%)	24	48.0	72.0
	48	26.0	39.0
	72	31.0	46.5
ZIF-8A(74%)	24	14.0	21.0
	48	18.0	27.0
	72	13.0	19.5

Table 2. DEE(%) and DLC(%) for prepared MOFs.

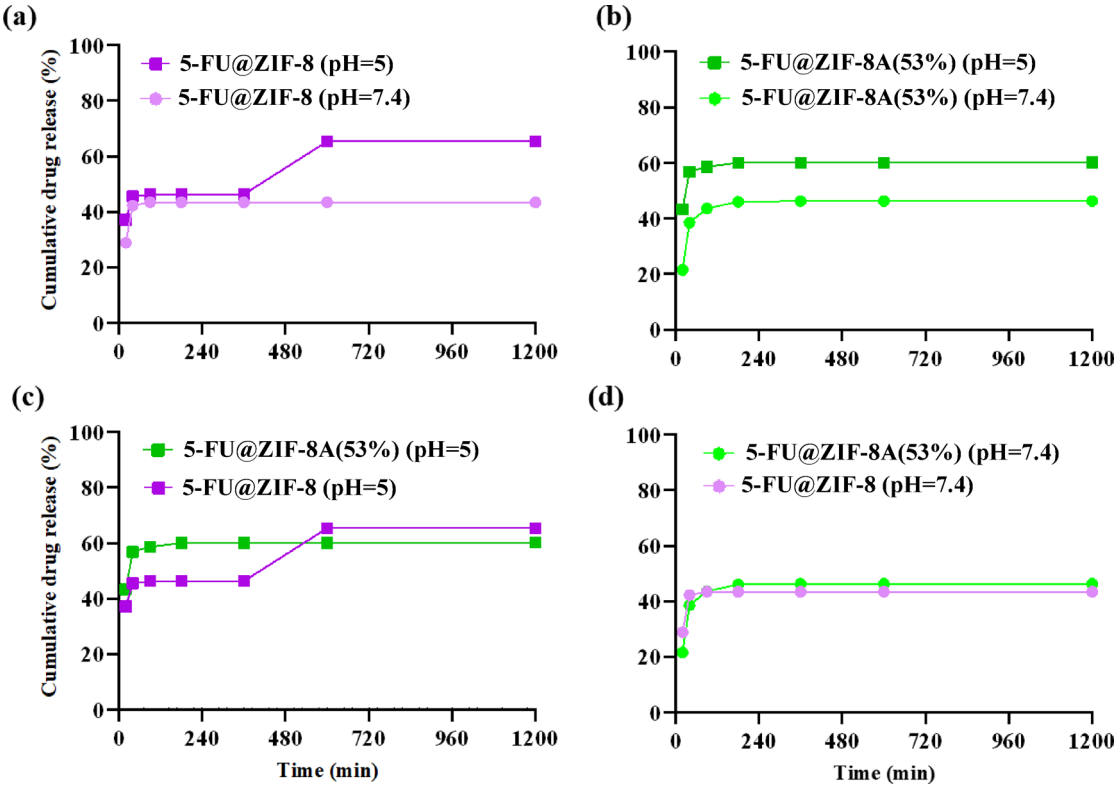

Fig. 4. Drug release profile of (**a**) 5-FU@ZIF-8 and (**b**) 5-FU@ZIF-8A(53%) in pH 5 and 7.4, and (**c**) 5-FU@ZIF-8 and 5-FU@ZIF-8A(53%) in pH 5, and (**d**) 5-FU@ZIF-8 and 5-FU@ZIF-8A(53%) in pH 7.4.

on both cell lines. Also, a similar concentration range of ZIF-8 and ZIF-8A(53%) was tested on a normal cell line. Additionally, MTT assay was performed for free 5-FU at concentrations of 0.5–100 µg/mL to compare the cytotoxicity of samples with 5-FU towards the cancer cells. It is evident from Fig. 5 that all samples showed a time- and dose-dependent cytotoxic effect by reduced cell proliferation and viability. For the MCF-7 cell line, IC50 values of 5-FU@ZIF-8A(53%) at 24 and 48 h were 18.42 and 7.929 µg/mL, respectively, while for 5-FU@ZIF-8, the IC50 values were slightly higher at 21.36 and 6.235 µg/mL (Fig. 5a,b). This suggests that 5-FU@ZIF-8A(53%) nanocarrier exhibited higher cytotoxicity compared to 5-FU@ZIF-8 at 24 h. For free 5-FU, the IC50 values were calculated as 62.84 µg/mL and 4.353 µg/mL after 24 and 48 h of treatment for the MCF-7 cell line (Fig. S5). These results confirm that both mentioned nanocarriers exhibit significantly higher anticancer activity compared to free 5-FU after 24 h. The cell viability profiles of both nanocarriers in HFF-2 cell lines are illustrated in Fig. 5c, d demonstrating their comparatively lower cytotoxicity against normal cells compared to cancer cells. The cell viability for the 5-FU@ZIF-8A(53%) nanocarrier at a concentration of 18.42 µg/mL was approximately 70% in the HFF-2 cell line. However, at a concentration of 21.36 µg/mL, the cell viability for the 5-FU@ZIF-8 nanocarrier was around 60% in the HFF-2 cell line. Based on these findings, it can be concluded that at the same level of cell growth inhibition in cancer cells, 5-FU@ZIF-8A(53%) exhibits lower cytotoxicity in normal cells compared to 5-FU@ZIF-8. This indicates that 5-FU@ZIF-8A(53%) has higher biocompatibility while maintaining its effectiveness against cancer cells. Moreover, Figs. 5e, f illustrate the cell viability of ZIF-8 and ZIF-8A(53%) toward the HFF-2 cell line after 24 and 48 h. According to ISO 10993-5, materials with cell viability above 70% are considered biocompatible[68]. The pristine ZIF-8 and ZIF-8A(53%) demonstrate acceptable cell viability up to a threshold value of 20 and 50 µg/mL after 24 h, respectively. The decreased cell viability was observed for both nanoparticles after 48 h. Based on these results, the ZIF-8A(53%) exhibits less cytotoxicity toward the normal cell line compared to ZIF-8 up to 50 µg/mL. Furthermore, it has been proven that 5-FU is quickly taken up by cells through the uracil transporter. To exert its cytotoxic properties, 5-FU is converted intracellularly into three active metabolites: fluorodeoxyuridine triphosphate (FdUTP), fluorodeoxyuridine monophosphate (FdUMP), and fluorouridine triphosphate (FUTP) which are responsible for the 5-FU antineoplastic activity. These metabolites inhibit the nucleotide synthetic enzyme TS and RNA synthesis[69]. Interestingly, previous studies have proposed that the major cytotoxicity mechanism of 5-FU in the MCF-7 cell line is its incorporation into RNA[70]. Also, it is established that the active metabolites of 5-FU, FdUTP and FUTP, are incorporated into DNA and RNA[71,72]. Incorporation into RNA disrupts the synthesis and processing of critical RNA molecules, including mRNAs, tRNAs, and rRNAs[73,74].

Table 3 presents a comparative analysis of different MOFs utilized for 5-FU drug delivery. Among the evaluated MOFs, ZIF-8A(53%) demonstrates favorable performance in terms of drug loading efficiency, drug release, and cell viability. Although other MOFs display potential advantages in certain areas, they also face specific limitations that may require further optimization. For instance, bi-MIL-88B[75] and Fe-MIL-53-NH_2[76]

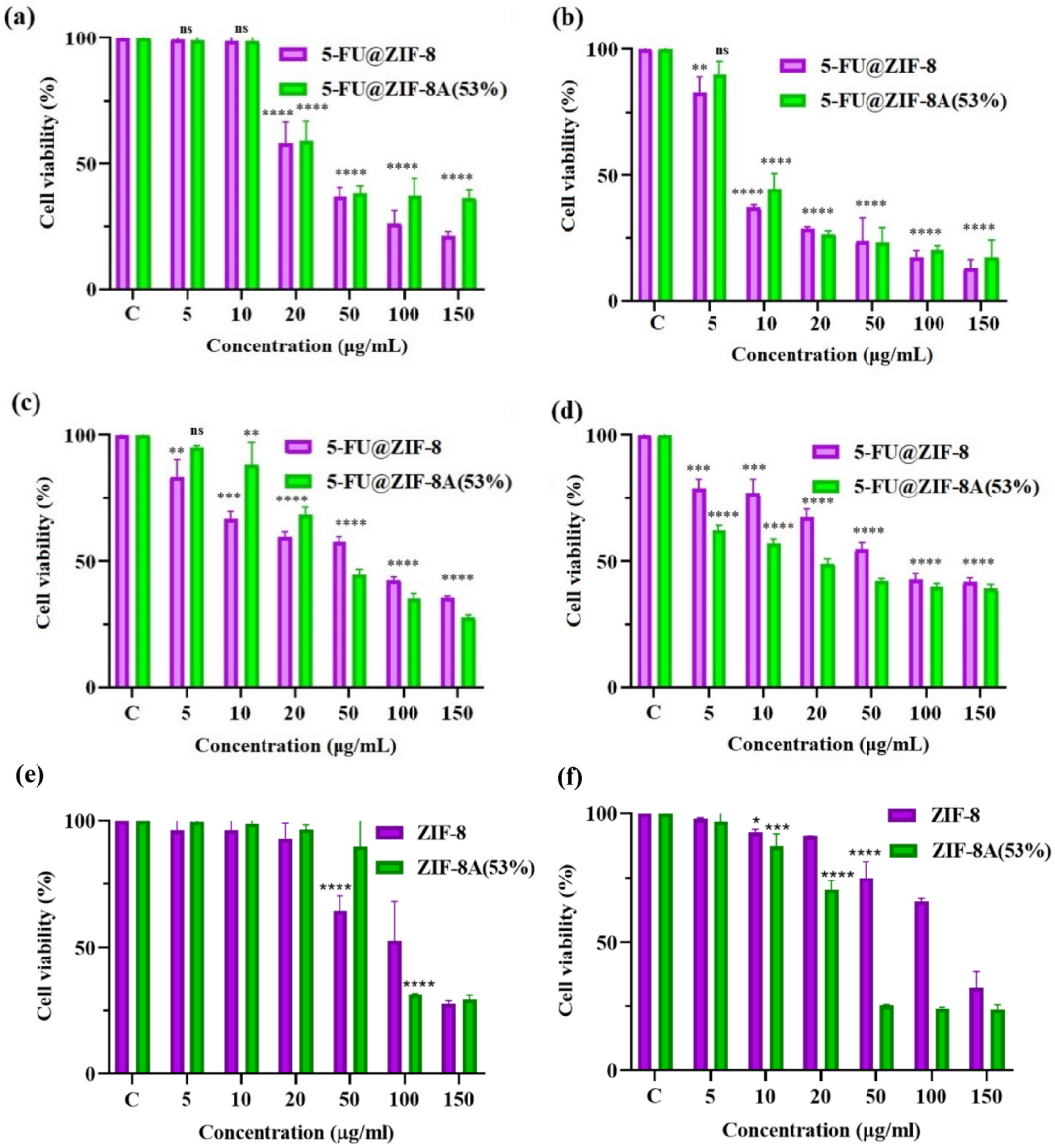

Fig. 5. Cell viability of 5-FU@ZIF-8 and 5-FU@ZIF-8A(53%) on MCF-7 cell line after (**a**) 24 h and (**b**) 48 h, and on HFF-2 cell line after (**c**) 24 h and (**d**) 48 h, and ZIF-8 and ZIF-8A(53%) on HFF-2 cell line after (**e**) 24 h and (**f**) 48 h. Results were considered statistically significant at the *p*-value of < 0.01 (**), < 0.001(***), < 0.0001(****) and ns: no significant.

systems encounter challenges related to low drug encapsulation and complex synthesis processes. The α-Fe_2O_3 nanoplates/AlFu MOF nanosheets[77] exhibited improved drug loading and release characteristics; however, the presence of magnetic α-Fe_2O_3 in DDS without further coating posing challenges, such as the potential for generating harmful free radicals under physiological conditions, which may lead to oxidative stress and damage to surrounding healthy tissues[78]. Moreover, Zn-MOF@GO[79] and Fe_3O_4@UiO-66-NH_2[80] demonstrated a relatively lower drug release percentage in an acidic environment. Incorporating magnetic Fe_3O_4 in UiO-66-NH_2 DDS introduced similar drawbacks as mentioned for α-Fe_2O_3, raising concerns about long-term toxicity. Also, copper-based MOF (HKUST-1)[81] showed a relatively high drug release percentage under neutral conditions, which may limit its therapeutic efficiency. The Dy(III)-MOF[82] system showed low drug encapsulation, and the partial decomposition of structure in an acidic environment may increase the risk of side effects due to the Dy^{3+} ions, which can accumulate in certain organs[83]. The folic acid modification in MOF-808[84] resulted in more effective drug delivery for cancerous tissue; however, it may cause off-target effects due to the expression of folic receptors in various normal tissues (as discussed in the Introduction section). Compared to other MOFs, ZIF-8A(53%) stands out with its favorable performance for 5-FU, especially in drug loading efficiency (except entry 3), pH-responsive sustained release, and selective cytotoxicity against cancer cells. While its cytotoxicity toward normal cells is not the lowest among others, it remains within an acceptable range and does not compromise its significant advantages. These findings highlight ZIF-8A(53%) as a cost-effective and highly promising

MOF	Modification	Major components	5-FU loading efficiency (%)	Drug release (%) at different pH	Cell line	MTT assay result	Ref
bi-MIL-88B	Coated by FA-conjugated chitosan	Fe^{3+}, Co^{2+}, Terephthalic acid (H_2BDC), Folic acid (FA), chitosan	18.2	58 at pH 5.2 24.9 at pH 7.4	HEK-293	N.A	75
					SW480	IC50 of 136 µg/mL-48 h	
Fe-MIL-53- NH_2	Modified by FA and FAM	Fe^{3+}, 2-amino terephthalic acid (NH_2-H_2BDC), FA, 5-carboxyl fluorescein (FAM)	23	–	MGC-803	45% cell viability-48 h	76
					HASMC	80% cell viability-48 h	
α-Fe_2O_3/AlFu MOF	–	Al^{3+}, Fumaric acid, α-Fe_2O_3	65	88.8 at pH 5 59.8 at pH 7.4	BT-20	55.8% cell viability-48 h	77
Zn-MOF@GO	Coated by chitosan	Zn^{2+}, H_2BDC, graphene oxide, chitosan	45	40 at pH 5 20 at pH 7.4	MDA-MB 231	41.2% cell viability-48 h	79
Fe_3O_4@UiO-66-NH_2	Coated by WP6	Zr^{4+}, NH_2-H_2BDC, Fe_3O_4, carboxylatopillar[6]arene (WP6)	30	20 at pH 5 12.5 at pH 7	Hella	85% cell viability-24 h	80
					HUVEC	100% cell viability-24 h	
HKUST-1	–	Cu^{2+}, benzene 1,3,5- tricarboxylic acid (H_3BTC)	40.23	60 at pH 7.4	HepG2	38% cell viability-48 h	81
Dy(III)-MOF	–	Dy3 + , 1,3,5-bezenetricarboxylate (BTC)	20.6	78 at pH 5 50 at pH 7.4	SF17	60% cell viability-24 h	82
					HASM	92% cell viability-24 h	
MOF-808	Modified by FA	Zr^{4+}, BTC	38.42	70 at pH 5.5 45 at pH 7.4	Hella	60% cell viability-24 h	84
					L-929	80% cell viability-24 h	
ZIF-8A(53%)	–	Zn^{2+}, 3-amino-1,2,4-triazole (Atz), 2-methylimidazole (2-MIM)	48	60 at pH 5 46 at pH 7.4	MCF-7	50% cell viability-24 h	This work
					HFF-2	70% cell viability-24 h	

Table 3. Comparison of different MOFs for 5-FU drug delivery. *N.A* not accountable.

nanocarrier for further development. In future studies, we aim to introduce more biocompatible linkers to minimize the cytotoxicity while maintaining its remarkable drug delivery properties.

Conclusions

In conclusion, ZIF-8 and ZIF8-A nanoparticles with different percentages of Atz exchange were successfully synthesized using the SALE method, and their performance as 5-FU carriers was evaluated. Our results revealed that ZIF-8A(53%) exhibited a notable drug encapsulation efficiency of 48%, significantly higher than ZIF-8 with only 12%. Additionally, a slower pH-responsive release was observed for 5-FU@ZIF-8A(53%) compared to 5-FU@ZIF-8. These findings suggest that the amine functional group in ZIF-8A(53%) increases its affinity for 5-FU molecules, enhancing drug encapsulation efficiency and enabling controlled release. The MTT assay results showed that 5-FU@ZIF-8A(53%) has less cytotoxicity on normal cells compared to 5-FU@ZIF-8 at the optimal treatment dose. Moreover, the bare ZIF-8A(53%) exhibits more biocompatibility compared to ZIF-8 on normal cell line at low concertrations. The proposed SALE method for designing more effective DDS based on ZIF-8 is considered facile and cost-effective compared to the mentioned surface modification strategies. This study underscored the potential of ZIF-8A(53%) as an effective carrier for 5-FU delivery. The results revealed that ZIF-8A(53%) is a suitable nanocarrier for 5-FU, holding significant value for further *in-vivo* studies to explore its clinical applications. At the same time, its potential as a nanocarrier for other small drugs is also worth investigating.

Data availability

Data is provided within the manuscript or supplementary information files.

Received: 31 December 2024; Accepted: 21 May 2025
Published online: 29 May 2025

References

1. Wang, Q.-Q., Yang, Z.-P., Cui, Z.-T., Wang, X.-H. & Lin, Y. A microporous Co(II)-MOF as a pH-responsive 5-Fu delivery system to induce human hemangioma cells apoptosis and abrogate their growth. *J. Coord. Chem.* **73**, 1436–1449 (2020).
2. Xiao, X. et al. Core–shell structured 5-FU@ ZIF-90@ ZnO as a biodegradable nanoplatform for synergistic cancer therapy. *Nanoscale* **12**, 3846–3854 (2020).
3. Sethy, C. & Kundu, C. N. 5-Fluorouracil (5-FU) resistance and the new strategy to enhance the sensitivity against cancer: Implication of DNA repair inhibition. *Biomed. Pharmacother.* **137**, 111285 (2021).
4. Azevedo, A. et al. An alternative hybrid lipid nanosystem combining cytotoxic and magnetic properties as a tool to potentiate antitumor effect of 5-fluorouracil. *Life Sci.* **344**, 122558 (2024).
5. Ji, X., Yang, Z., Fang, J. & Hu, S. Molecularly imprinted polymers based on attapulgite and sustained-release properties for 5-FU. *Colloid Polym. Sci.* **302**, 1–10 (2024).
6. Salazar, J. et al. UiO-66(Zr) as drug delivery system for non-steroidal anti-inflammatory drugs. *J. Control. Release* **370**, 392–404 (2024).
7. Tibbitt, M. W., Dahlman, J. E. & Langer, R. Emerging Frontiers in Drug Delivery. *J. Am. Chem. Soc.* **138**, 704–717 (2016).
8. Mandal, A., Dhineshkumar, E. & Murugan, E. Collagen biocomposites derived from fish waste: Doped and cross-linked with functionalized Fe3O4 nanoparticles and their comparative studies with a green approach. *ACS Omega* **8**, 24256–24267 (2023).

9. Mandal, A., Sekar, S., Chandrasekaran, N., Mukherjee, A. & Sastry, T. P. Synthesis, characterization and evaluation of collagen scaffolds crosslinked with aminosilane functionalized silver nanoparticles: in vitro and in vivo studies. *J. Mater. Chem. B* **3**, 3032–3043 (2015).
10. Mandal, A., Dhineshkumar, E. & Sastry, T. The CCLW collagen biocomposite consisting Ag–Fe_3O_4 nanoparticles as a novel biomaterial with a view to facile green approach. *Clean Technol. Environ. Policy* **25**, 3285–3302 (2023).
11. Pederneira, N., Aina, P. O., Rownaghi, A. A. & Rezaei, F. Performance of MIL-101(Cr) and MIL-101(Cr)-pore expanded as drug carriers for ibuprofen and 5-fluorouracil delivery. *ACS Appl. Bio Mater.* **7**, 1041–1051 (2024).
12. Prasetya, N. & Ladewig, B. P. New Azo-DMOF-1 MOF as a photoresponsive low-energy CO_2 adsorbent and its exceptional CO_2/N_2 separation performance in mixed matrix membranes. *ACS Appl. Mater. Interfaces.* **10**, 34291–34301 (2018).
13. Gu, X.-W. et al. Immobilization of Lewis basic sites into a stable ethane-selective MOF enabling one-step separation of ethylene from a ternary mixture. *J. Am. Chem. Soc.* **144**, 2614–2623 (2022).
14. Chen, L.-W. et al. Metal-organic framework membranes encapsulating gold nanoparticles for direct plasmonic photocatalytic nitrogen fixation. *J. Am. Chem. Soc.* **143**, 5727–5736 (2021).
15. Li, W. et al. Rational design and general synthesis of multimetallic metal-organic framework nano-octahedra for enhanced Li–S battery. *Adv. Mater.* https://doi.org/10.1002/adma.202105163 (2021).
16. Gorai, T., Schmitt, W. & Gunnlaugsson, T. Highlights of the development and application of luminescent lanthanide based coordination polymers, MOFs and functional nanomaterials. *Dalton Trans.* **50**, 770–784 (2021).
17. El-Bindary, M. A., El-Desouky, M. G. & El-Bindary, A. A. Metal–organic frameworks encapsulated with an anticancer compound as drug delivery system: Synthesis, characterization, antioxidant, anticancer, antibacterial, and molecular docking investigation. *Appl. Organomet. Chem.* **36**, e6660 (2022).
18. Wang, Y. et al. Metal-organic frameworks for stimuli-responsive drug delivery. *Biomaterials* **230**, 119619 (2020).
19. Le, B. T., La, D. D. & Nguyen, P. T. H. Ultrasonic-assisted fabrication of MIL-100(Fe) metal-organic frameworks as a carrier for the controlled delivery of the chloroquine drug. *ACS Omega* **8**, 1262–1270 (2023).
20. Chen, J. et al. Titanium-based metal-organic frameworks as pH-responsive drug delivery carriers of 5-fluorouracil. *J. Solid State Chem.* **332**, 124563 (2024).
21. Bagherzadeh, M., Chegeni, M., Bayrami, A. & Amini, M. Superior and efficient performance of cost-effective MIP-202 catalyst over UiO-66-$(CO_2H)_2$ in epoxide ring opening reactions. *Sci. Rep.* **14**, 17730 (2024).
22. Pooresmaeil, M., Åsl, E. A. & Namazi, H. A new pH-sensitive CS/Zn-MOF@ GO ternary hybrid compound as a biofriendly and implantable platform for prolonged 5-fluorouracil delivery to human breast cancer cells. *J. Alloy. Compd.* **885**, 160992 (2021).
23. Lee, Y. R., Do, X. H., Cho, K. Y., Jeong, K. & Baek, K.-Y. Amine-functionalized zeolitic imidazolate framework-8 (ZIF-8) Nanocrystals for adsorption of radioactive iodine. *ACS Appl. Nano Mater.* **3**, 9852–9861 (2020).
24. Sun, C.-Y. et al. Zeolitic imidazolate framework-8 as efficient pH-sensitive drug delivery vehicle. *Dalton Trans.* **41**, 6906–6909 (2012).
25. Shi, Q., Chen, Z., Song, Z., Li, J. & Dong, J. Synthesis of ZIF-8 and ZIF-67 by steam-assisted conversion and an investigation of their tribological behaviors. *Angew. Chem. Int. Ed.* **50**, 672–675 (2011).
26. Bagherzadeh, M., Bayrami, A., Shekari, Z. & Amini, M. High-performance thin-film nanocomposite (TFN) forward osmosis (FO) membranes incorporated with porous hydrophobic-core/hydrophilic-shell nanoparticles. *Desalination* **515**, 115181 (2021).
27. Zheng, H. et al. One-pot synthesis of metal–organic frameworks with encapsulated target molecules and their applications for controlled drug delivery. *J. Am. Chem. Soc.* **138**, 962–968 (2016).
28. Zeng, Y. et al. Current status and prospect of ZIF-based materials for breast cancer treatment. *Colloids Surf., B* **232**, 113612 (2023).
29. Yan, J. et al. Mineralization of pH-sensitive doxorubicin prodrug in ZIF-8 to enable targeted delivery to solid tumors. *Anal. Chem.* **92**, 11453–11461 (2020).
30. Chen, P., He, M., Chen, B. & Hu, B. Size- and dose-dependent cytotoxicity of ZIF-8 based on single cell analysis. *Ecotoxicol. Environ. Saf.* **205**, 111110 (2020).
31. Peng, L. et al. Preparation of PEG/ZIF-8@ HF drug delivery system for melanoma treatment via oral administration. *Drug Del.* **29**, 1075–1085 (2022).
32. Wang, Q. et al. ZIF-8 integrated with polydopamine coating as a novel nano-platform for skin-specific drug delivery. *J. Mater. Chem. B* **11**, 1782–1797 (2023).
33. Yu, S. et al. Hyaluronic acid coating on the surface of curcumin-loaded ZIF-8 nanoparticles for improved breast cancer therapy: An in vitro and in vivo study. *Colloids Surf., B* **203**, 111759 (2021).
34. Ren, S.-Z. et al. Nanoscale metal–organic-frameworks coated by biodegradable organosilica for pH and redox dual responsive drug release and high-performance anticancer therapy. *ACS Appl. Mater. Interfaces* **11**, 20678–20688 (2019).
35. Wu, Q. et al. Biocompatible and biodegradable zeolitic imidazolate framework/polydopamine nanocarriers for dual stimulus triggered tumor thermo-chemotherapy. *Biomaterials* **162**, 132–143 (2018).
36. Su, L. et al. High biocompatible ZIF-8 Coated by ZrO_2 for chemo-microwave thermal tumor synergistic therapy. *ACS Appl. Mater. Interfaces* **11**, 10520–10531 (2019).
37. Wang, Q., Sun, Y., Li, S., Zhang, P. & Yao, Q. Synthesis and modification of ZIF-8 and its application in drug delivery and tumor therapy. *RSC Adv.* **10**, 37600–37620 (2020).
38. Oryani, M. A. et al. Targeted cancer treatment using folate-conjugated sponge-like ZIF-8 nanoparticles: A review. *Naunyn Schmiedebergs Arch. Pharmacol.* **397**, 1377–1404 (2024).
39. Reshmi, R., Jiju, K. R., Suma, S. & Anoop, S. N. Folic acid grafted aminated zeolitic imidazolate framework (ZIF-8) as pH responsive drug carrier for targeted delivery of curcumin. *J. Drug Del. Sci. Technol.* **79**, 104098 (2023).
40. Chinnathambi, A., Alharbi, S. A., Ramar, M., Arulselvan, P. & Muthusami, S. Fabrication of folic acid-embedded aminated drug encapsulated zeolitic imidazolate framework as promising drug delivery system for lung cancer. *J. Mater. Res.* **39**(10), 1537–1547 (2024).
41. Agnello, L., Camorani, S., Fedele, M. & Cerchia, L. Aptamers and antibodies: rivals or allies in cancer targeted therapy?. *Explor. Target. Anti-tumor Therapy* **2**, 107 (2021).
42. Liu, Y., Yang, G., Jin, S., Xu, L. & Zhao, C. X. Development of high-drug-loading nanoparticles. *ChemPlusChem* **85**, 2143–2157 (2020).
43. Deria, P. et al. Beyond post-synthesis modification: evolution of metal–organic frameworks via building block replacement. *Chem. Soc. Rev.* **43**, 5896–5912 (2014).
44. Shi, Z. et al. FA-PEG decorated MOF nanoparticles as a targeted drug delivery system for controlled release of an autophagy inhibitor. *Biomaterials science* **6**, 2582–2590 (2018).
45. Yin, X. et al. Polydopamine-modified ZIF-8 nanoparticles as a drug carrier for combined chemo-photothermal osteosarcoma therapy. *Colloids Surf., B* **216**, 112507 (2022).
46. Zhao, H. et al. Development of novel paclitaxel-loaded ZIF-8 metal-organic framework nanoparticles modified with peptide dimers and an evaluation of its inhibitory effect against prostate cancer cells. *Pharmaceutics* **15**, 1874 (2023).
47. Esfahanian, M., Ghasemzadeh, M. A. & Razavian, S. M. H. Synthesis, identification and application of the novel metal-organic framework Fe_3O_4@ PAA@ ZIF-8 for the drug delivery of ciprofloxacin and investigation of antibacterial activity. *Artific. Cells Nanomed. Biotechnol.* **47**, 2024–2030 (2019).
48. Pham, T. Q. et al. Nanoscale ZIF-8 as an efficient carboplatin carrier for targeted cancer therapy. *Inorg. Chem. Commun.* **165**, 112567 (2024).

49. Cho, K. Y. et al. Synthesis of amine-functionalized ZIF-8 with 3-amino-1,2,4-triazole by postsynthetic modification for efficient CO_2-selective adsorbents and beyond. *J. Mater. Chem. A* **6**, 18912–18919 (2018).
50. Lee, Y.-R., Do, X. H., Hwang, S. S. & Baek, K.-Y. Dual-functionalized ZIF-8 as an efficient acid-base bifunctional catalyst for the one-pot tandem reaction. *Catal. Today* **359**, 124–132 (2021).
51. Ray Chowdhuri, A., Laha, D., Pal, S., Karmakar, P. & Sahu, S. One-pot synthesis of folic acid encapsulated upconversion nanoscale metal organic frameworks for targeting, imaging and pH responsive drug release. *Dalton Trans.* **45**, 18120–18132 (2016).
52. Paswan, S. K. & Saini, T. Comparative evaluation of in vitro drug release methods employed for nanoparticle drug release studies. *Clin. Trials* **14**, 17 (2021).
53. Kim, Y., Park, E. J., Kim, T. W. & Na, D. H. Recent progress in drug release testing methods of biopolymeric particulate system. *Pharmaceutics* **13**, 1313 (2021).
54. Nabipour, H., Aliakbari, F., Volkening, K., Strong, M. J. & Rohani, S. The development of a bio-based metal-organic framework coated with carboxymethyl cellulose with the ability to deliver curcumin with anticancer properties. *Mater. Today Chem.* **37**, 101976 (2024).
55. Li, G.-L. et al. Recyclable dehydrogenation/regeneration of ammonia borane nanoconfined in amino-functionalized ZIF-8 with 3-amino-1,2,4-triazole. *ACS Sustain. Chem. Eng.* **11**, 6143–6152 (2023).
56. Bagherzadeh, M. & Mesbahi, E. Heterogenization of manganese porphyrin via hydrogen bond in zeolite imidazolate framework-8 matrix, a host–guest interaction, as catalytic system for olefin epoxidation. *J. Porphyrins Phthalocyanines* **22**, 972–980 (2018).
57. Padya, B. S. et al. Targeted delivery of 5-Fluorouracil and sonidegib via surface-modified ZIF-8 MOFs for effective basal cell carcinoma therapy. *Pharmaceutics* **15**, 2594 (2023).
58. Chiñas-Rojas, L. E. et al. Exploring synthesis strategies and interactions between MOFs and drugs for controlled drug loading and release, characterizing interactions through advanced techniques. *ChemMedChem* **19**, e202400144 (2024).
59. Ahmed, I. & Jhung, S. H. Applications of metal-organic frameworks in adsorption/separation processes via hydrogen bonding interactions. *Chem. Eng. J.* **310**, 197–215 (2017).
60. Mohammadi, A. & NakhaeiPour, A. Triethylenetetramine-impregnated ZIF-8 nanoparticles for CO_2 adsorption. *J. CO2 Util.* **69**, 102424 (2023).
61. Parsaei, M. & Akhbari, K. MOF-801 as a nanoporous water-based carrier system for in situ encapsulation and sustained release of 5-FU for effective cancer therapy. *Inorg. Chem.* **61**, 5912–5925 (2022).
62. Almáši, M., Zeleňák, V., Palotai, P., Beňová, E. & Zeleňáková, A. Metal-organic framework MIL-101(Fe)-NH_2 functionalized with different long-chain polyamines as drug delivery system. *Inorg. Chem. Commun.* **93**, 115–120 (2018).
63. Zhou, Z., Ke, Q., Wu, M., Zhang, L. & Jiang, K. Pore space partition approach of ZIF-8 for pH responsive codelivery of ursolic acid and 5-fluorouracil. *ACS Mater. Lett.* **5**, 466–472 (2023).
64. Silva, J. S. F. et al. Multifunctional system polyaniline-decorated ZIF-8 nanoparticles as a new chemo-photothermal platform for cancer therapy. *ACS Omega* **3**, 12147–12157 (2018).
65. Ebadi, M., Buskaran, K., Bullo, S., Fakurazi, S. & Hussein, M. the impact of magnesium–aluminum-layered double hydroxide-based polyvinyl alcohol coated on magnetite on the preparation of core-shell nanoparticles as a drug delivery agent. *Int. J. Mol. Sci.* **20**, 3764 (2019).
66. Abánades Lázaro, I. et al. Metal–organic frameworks for biological applications. *Nat. Rev. Methods Prim.* **4**, 42 (2024).
67. Jiao, G. et al. Limitations of MTT and CCK-8 assay for evaluation of graphene cytotoxicity. *RSC Adv.* **5**, 53240–53244 (2015).
68. Lagonegro, P. et al. A cytotoxicity study of silicon oxycarbide nanowires as cell scaffold for biomedical applications. *Mater. Sci. Eng., C* **73**, 465–471 (2017).
69. Ciaffaglione, V. et al. Mutual prodrugs of 5-fluorouracil: From a classic chemotherapeutic agent to novel potential anticancer drugs. *ChemMedChem* **16**, 3496–3512 (2021).
70. Kufe, D. W. & Major, P. P. 5-Fluorouracil incorporation into human breast carcinoma RNA correlates with cytotoxicity. *J. Biol. Chem.* **256**, 9802–9805 (1981).
71. Ghoshal, K. & Jacob, S. T. Specific inhibition of pre-ribosomal RNA processing in extracts from the lymphosarcoma cells treated with 5-fluorouracil. *Can. Res.* **54**, 632–636 (1994).
72. Aherne, G. W., Hardcastle, A., Raynaud, F. & Jackman, A. L. Immunoreactive dUMP and TTP pools as an index of thymidylate synthase inhibition; effect of tomudex (ZD1694) and a nonpolyglutamated quinazoline antifolate (CB30900) in L1210 mouse leukaemia cells. *Biochem. Pharmacol.* **51**, 1293–1301 (1996).
73. Kanamaru, R., Kakuta, H., Sato, T., Ishioka, C. & Wakui, A. The inhibitory effects of 5-fluorouracil on the metabolism of preribosomal and ribosomal RNA in L-1210 cells in vitro. *Cancer Chemother. Pharmacol.* **17**, 43–46 (1986).
74. Randerath, K., Tseng, W.-C., Harris, J. & Lu, L.-J. *in Modified Nucleosides and Cancer* 283–297 (Springer, 1983).
75. Akbar, M. U. et al. A pH-responsive bi-MIL-88B MOF coated with folic acid-conjugated chitosan as a promising nanocarrier for targeted drug delivery of 5-Fluorouracil. *Front. Pharmacol.* **14**, 1265440 (2023).
76. Gao, X. et al. Controllable synthesis of a smart multifunctional nanoscale metal–organic framework for magnetic resonance/optical imaging and targeted drug delivery. *ACS Appl. Mater. Interfaces* **9**, 3455–3462 (2017).
77. Ataee Khorrami, M., Sohrabnezhad, S. & Asadollahi, A. Synthesis and characterization of α-Fe_2O_3 nanoplates/aluminum fumarate metal-organic framework nanosheets as a nanocarrier for anticancer drug. *Mater. Today Chem.* **34**, 101777 (2023).
78. Pourmadadi, M. et al. Role of iron oxide (Fe_2O_3) Nanocomposites in advanced biomedical applications: A state-of-the-art review. *Nanomaterials* **12**, 3873 (2022).
79. Pooresmaeil, M., Asl, E. A. & Namazi, H. A new pH-sensitive CS/Zn-MOF@GO ternary hybrid compound as a biofriendly and implantable platform for prolonged 5-fluorouracil delivery to human breast cancer cells. *J. Alloy. Compd.* **885**, 160992 (2021).
80. Wu, M. X. et al. Multistimuli responsive core-shell nanoplatform constructed from Fe_3O_4 @MOF equipped with Pillar[6]arene nanovalves. *Small* **14**, e1704440 (2018).
81. Li, Y. et al. Strategy for chemotherapeutic delivery using a nanosized porous metal-organic framework with a central composite design. *Int. J. Nanomed.* **12**, 1465–1474 (2017).
82. Chen, L., Yu, H., Li, Y., Zhang, X. & Du, Y. Fabrication of a microporous Dy(III)-organic framework with polar channels for 5-Fu (fluorouracil) delivery and inhibiting human brain tumor cells. *Struct. Chem.* **29**, 1885–1891 (2018).
83. Pałasz, A. & Czekaj, P. Toxicological and cytophysiological aspects of lanthanides action. *Acta Biochim. Pol.* **47**, 1107–1114 (2000).
84. Dong, H. et al. Folic acid functionalized zirconium-based metal–organic frameworks as drug carriers for active tumor-targeted drug delivery. *Chem.: Eur. J.* **24**, 17148–17154 (2018).

Acknowledgements

Support of this study by the Sharif University of Technology Research Council is gratefully acknowledged.

Author contributions

Sahba Mirzanejad: Formal analysis; investigation; methodology; resources; validation; writing original draft; writing-review and editing. Mojtaba Bagherzadeh: Conceptualization; project administration; supervision; review and editing. Arshad Bayrami: Investigation; supervision; writing-review and editing. Hossein Daneshgar: Investigation, review and editing. Aida Bahrami: Investigation. Majid Mahdavi: Investigation, review and ed-

iting.

Declarations

Competing interests
The authors declare no competing interests.

Additional information
Supplementary Information The online version contains supplementary material available at https://doi.org/10.1038/s41598-025-03542-2.

Correspondence and requests for materials should be addressed to M.B.

Reprints and permissions information is available at www.nature.com/reprints.

Publisher's note Springer Nature remains neutral with regard to jurisdictional claims in published maps and institutional affiliations.